Tetrahedron 65 (2009) 5760–5766

Contents lists available at ScienceDirect

Tetrahedron

journal homepage: www.elsevier.com/locate/tet

Theoretical studies of azapentalenes. Part 4: Theoretical study of the properties of 3a,6a-diazapentalene

Ibon Alkorta, Fernando Blanco *, José Elguero

Instituto de Química Médica, CSIC, Juan de la Cierva, 3, E-28006 Madrid, Spain

ARTICLE INFO

Article history:
Received 24 February 2009
Received in revised form 5 May 2009
Accepted 7 May 2009
Available online 13 May 2009

Keywords:
Pentalenes
Aromaticity
Protonation
Hydrogen bonds
Stacking

ABSTRACT

A theoretical study of the properties of the isolated 3a,6a-diazapentalene by means of DFT, B3LYP/6-311++G(d,p) and ab initio methods, MP2/6-311++G(d,p), has been carried out. In addition, the complexes formed with hydrogen bond donor, acceptors, cations, and anions have been studied and analyzed. Ring opening into 1,5-diazocine as well as basicity and acidity properties of 3a,6a-diazapentalene have been explored. Their ability to form HB complexes and the complexes formed with anions and cations have been studied.

1. Introduction

Ring system **1** is known by different names: 1*H*-pyrazolo[1,2-*a*]pyrazol-4-ium hydroxide inner salt (1*H*-pyrazolo[1,2-*a*]pyrazol-8-ium hydroxide inner salt),[1] 3a,6a-diazapentalene **1a** (as a derivative of **2**),[2] and 1*H*-pyrazolo[1,2-*a*]pyrazol-8-ium-4-ide.[3] The compound is also represented with positive and negative charges delocalized in the aromatic system **1a** (Scheme 1). Note that due to the different names, **1** has two CAS Register Numbers, 7659-87-2 and 52916-57-1. According to Ramsden classification, the compound belongs to the family of mesomeric betaines.[4]

This ring system was discovered simultaneously by Solomons[5] and by Trofimenko[6] who reported the preparation, chemical reactivity and some spectroscopic properties of the parent system and some of its derivatives. We have contributed with a ^{1}H and ^{13}C NMR study of these systems,[7] that continues to be studied (mainly for their chemical and biological properties).[8–10] Theoretical studies on these systems are scarce, in the paper already cited[7] we reported AM1 calculation on **1**. Other authors carried out ASMO-SCF-CI semiempirical calculations on **1** and other related heterocycles,[11] and there is a review on mesoionic heterocycles and heterocyclic betaine cations that includes **1** and its *C*-substituted derivatives.[12]

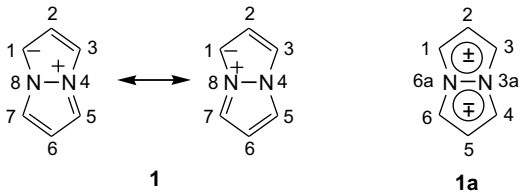

Scheme 1. Representations of compound **1**.

2. Results and discussion

This section has been divided in different parts, focusing the first one (section 2.1) in the static properties of **1**, as those derived from their geometry, electronic distribution, and spectroscopic (UV, IR, and NMR) characteristics. After, the mechanism of the ring-chain isomerism (section 2.2) and acid-base (sections 2.3 and 2.4) properties of **1** has been explored. Finally, the ability of **1** to form neutral hydrogen bonded complexes (section 2.5) and complexate with cations and anions (section 2.6) have been studied. In all cased B3LYP/6-311++G(d,p) and MP2/6-311++G(d,p) levels (see Methods section) have been used to properly characterize all these properties.

2.1. Properties of the isolated molecule: UV, IR, and NMR (GIAO and NICS)

Compound **1** is a small molecule with high-symmetry (D_{2h}) for which interesting properties are expected. A search on the CSD

* Corresponding author.
E-mail address: fblanco@iqm.csic.es (F. Blanco).

0040-4020/$ – see front matter © 2009 Elsevier Ltd. All rights reserved.
doi:10.1016/j.tet.2009.05.017

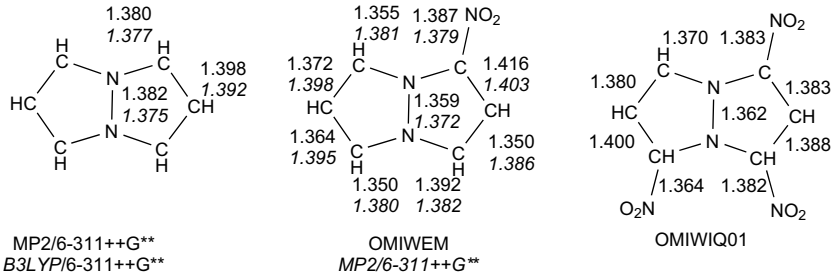

Scheme 2. Bond distances of the calculated and experimental derivatives of **1**. The CSD refcode of the systems is indicated.

database[13] for derivatives of **1** shows the presence of two nitro derivatives (OMIWIQ and OMIWEM) and a number of oxo derivatives (bimanes) that will not be considered in this article. The bond distances of these structures along those obtained in the calculations have been gathered in Scheme 2. Important effects are observed in the bond distances due to the presence of the nitro groups. For comparative purposes, the 1-nitro derivative OMIWEM has been calculated showing similar bond distances to the experimental ones.

The electrostatic potential of the isolated monomers presents the most negative regions above and below the C1–C2–C3 fragment (and the symmetric C4–C5–C6 one) and positive regions near the atomic positions, as expected for the interaction of a hypothetical positive charge and the atomic nucleus. The MEP minima are located approximately above and below the middle of each C–C bond (at 1.834 Å of C1 and 1.872 of C2), eight in the whole molecule, with a value of −0.030 a.u. calculated at the B3LYP/6-311++G(d,p) level.

These results preclude that the regions above and below the C1–C2–C3 moiety should be the receptor of electron demanding groups while those acting as electron donors will interact in the molecular plane with the hydrogen atoms (Fig. 1).

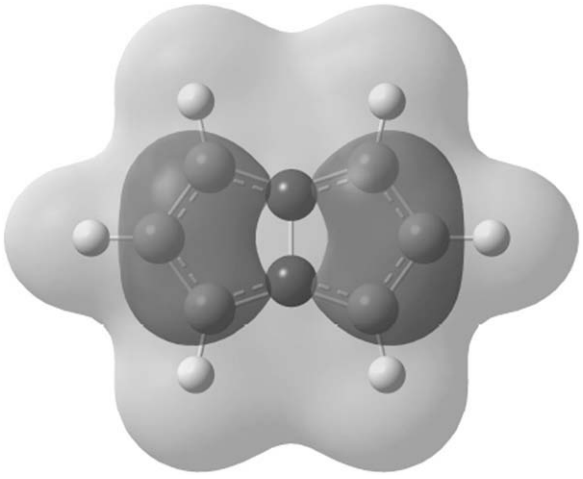

Figure 1. Electrostatic potential at ±0.02 a.u. isosurface. Dark regions correspond to negative electrostatic potential and light ones to positive values.

The Natural Resonance Theory (NRT) provides within the NBO methodology a quantitative analysis of the weight of the possible Lewis structures for a given molecule. The analysis for **1** led to a large family of contributing resonance forms. A representative sample of those structures with largest weight is shown in Figure 2. Due to the symmetry of the molecule, another three structures for each one of those represented in the figure, having the same weight, are obtained. Thus, the total contribution of those forms represents 70.6%. It is significant that the structures **B** and **C** with two positive and two negative charges are preferred over the **D** one with only one positive and a negative charge. Probably this is due to unfavorable location of the negative charge close to the lone pair of the neutral nitrogen atom in the resonance form **D**.

The Wiberg Bond indexes of **1** are 1.09 for N4–N8, 1.13 for N8–C1, and 1.45 for C1–C2 and related by symmetry bonds. These distances correspond to a distribution of the type **A** (Fig. 2) with a single N–N bond, three single and one double bond for N–C compared with two double and two single for C–C. These values are consistent with the ELF analysis (Fig. 3) that shows a disynaptic distribution in the C1–C2 bonds similar to those found in partial double bonds.[14]

The calculated UV spectrum, obtained using the TD-DFT methods, shows only one transition 287.1 nm with an oscillator strength of 0.259. It can be described as a transition between the HOMO to the LUMO^{+1}. The observed experimental value is λ_{max}=284 nm in deoxygenated EtOH 95%.[5d]

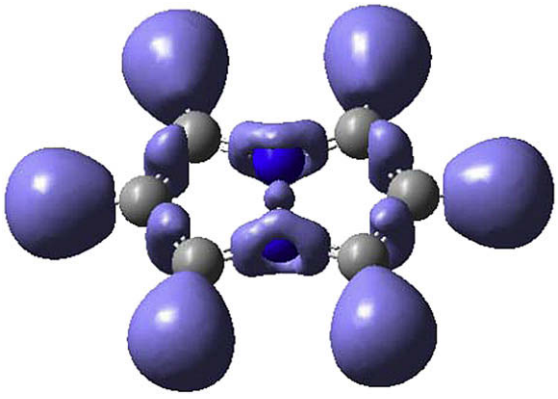

Figure 3. ELF isosurface with a value of 0.8.

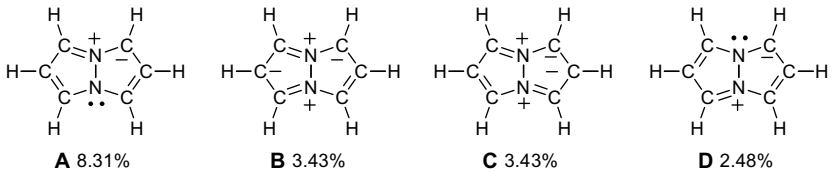

Figure 2. Most important structures found in the NRT analysis and their contribution. Due to the symmetry of the molecule, another three resonance forms are found for each case with the same contribution.

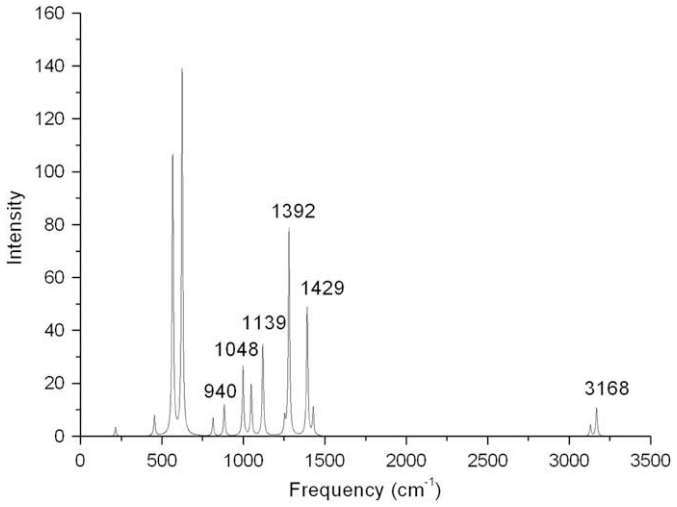

Figure 4. Scaled IR spectrum of **1**.

Table 1
Absolute chemical shieldings (σ, ppm) and NICS values calculated at the 3LYP/6-311++G(d,p) computational level

Atom	σ, ppm	δ, ppm	Exp.[5,6]	Molecule	NICS(0)	NICS(1)
N4	0.3633	−154.3	—	C_6H_6	−8.06	−10.23
C1	83.8334	95.0	—	**1**	−14.8	−9.94
C2	69.0024	109.3	—			
H1	24.9462	6.85	7.03±0.02			
H2	25.4082	6.39	6.57±0.08			

The calculated IR bands are shown in Figure 4. This spectrum must be compared with the experimental values (in Nujol under nitrogen): 3160 (s), 1430, 1400, 1139 (s), 1040, and 929 cm^{-1}.[6b] The 1400 band was reported at 1140 cm^{-1} in the older of the two Trofimenko's references.[6a] We have represented in Figure 4 the B3LYP/6-311++G(d,p) scaled values corresponding to equation Scaled (cm^{-1})=0.962* calculated (cm^{-1}), n=5, r^2=0.9998. The experimental 929 cm^{-1} band corresponds to two calculated bands centered, after scaling, at 940 cm^{-1}. The scaling factor, 0.962, is identical or close to those proposed recently for the same type of calculation (0.962 and 0.968).[15,16]

We report in Table 1 the calculated absolute chemical shieldings (σ) together with the corresponding δ values as well as the NICS values, all in parts per million.

To transform σ into δ we have used the following equations: δ^1H=31.8–1.00 σ^1H,[17] δ^{13}C=175.7–0.963 σ^{13}C,[18] and δ^{15}N=154.0–0.875 σ^{15}N.[18]

Taking into account that the experimental values were determined in DMSO, the signals of the protons are well reproduced. No information for the other nuclei is available, only the ^{1}H and ^{13}C NMR study of *C*-substituted derivatives of **1** has been reported.[7] Since there are data on some of these derivatives, we have calculated those of 1,3-dicyano-3a,6a-diazapentalene **2** (Scheme 3). The agreement is good enough to consider reliable the values predicted for **1**.

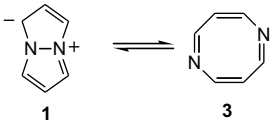

Scheme 4. Ring/ring isomerism of **1**.

Table 2
Isomerization energies

Isomer	B3LYP/6-311++G(d,p)	MP2/6-311++G(d,p)
	E_{rel} (kJ mol^{-1})	E_{rel} (kJ mol^{-1})
1	0.00	0.00
3	2.86	34.28
TS	127.42	175.16

The NICS values[19] at 0 Å are too sensitive to proximity effects (in the case of **1** it lies at the center of one of the five-member rings) but a 1 Å, compound **1** has an aromaticity similar to that of benzene. In azapentalenes lacking N atoms in positions 3a,6a, NICS(1)=9–11 ppm,[20] with only one N atom about 10 ppm,[21] and in the N_8 molecule (which has two N atoms in these positions), NICS(1)=12.8 ppm.[22]

2.2. Ring/ring isomerism

The ring/ring isomerism involving 1,5-diazocine **3** (Scheme 4) was suggested by Trofimenko in his paper describing the synthesis of **1**.[6b] He concludes that the aromatic 10π-electron azapentalene should be much more stable than the antiaromatic 8π-electron 1,5-diaza-cyclooctatetraene. This topic was discussed in several books,[2,23,24] but no progresses have been made in recent years. The analogous tetrahydroimidazo[4,5-*d*]imidazole systems has shown to present this isomerism, being the bicyclic structure more stable than the eight-member cyclic one.[25,26]

We have calculated the differences in energy between both isomers and located the corresponding TS (Table 2 and Fig. 5).

The structure of the TS shows an elongation of the N···N up to 2.347 Å at the MP2/6-311++ G(d,p) computational level while a bond path connecting both atoms is maintained (Fig. 5).

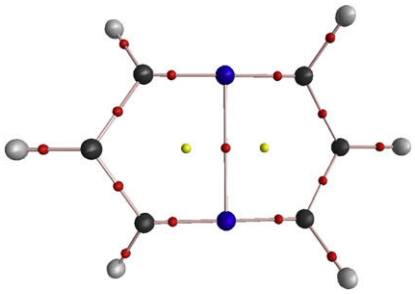

Figure 5. Molecular graph of the TS structure. The bond and ring critical points are shown with red and yellow balls, respectively. The bond paths connecting the atoms are shown.

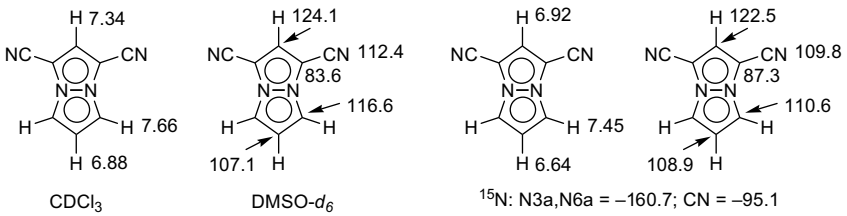

Scheme 3. Experimental (left) and calculated (right) ^{1}H and ^{13}C chemical shifts of compound **2**.

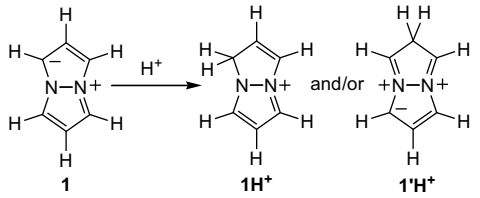

Scheme 5. Protonation of **1**.

2.3. Protonation

We described in a previous paper the protonation of **1** and related compounds bearing *C*-substituents by FAB mass spectrometry.[27] The resulting cation has the $\mathbf{1H}^+$ structure (Scheme 5). The calculations of Table 3 show that indeed C1 is the most basic position. This kind of cation when attacked by a strong base (LiH/DMSO) generates **1**.[5] The effect of the protonation on the carbon atoms over the geometry is limited to the ring where the proton is attached, while the other one is maintained almost unaltered. The larger effects are observed in the two C–C bonds surrounding the protonated carbon atom (Scheme 6).

2.4. Deprotonation

It is not known which is the most acidic C–H of **1** since no H/D exchange experiments in basic media have been reported (Scheme 7). It is known that **1** reacts with acetic anhydride, benzoyl chloride, and cyanogen chloride to give the 1,3-diacetyl, the 1,3-dibenzoyl, and the 1,3-dicyano derivative (**2**), respectively.[2] The results of Table 4 and Scheme 8 show that the C–H at positions 1 and 3 are much more acidic than that at C2. The geometrical effect of the deprotonation is much smaller than that found in the protonation and in general small changes in bond distances are observed (less than 0.03 Å).

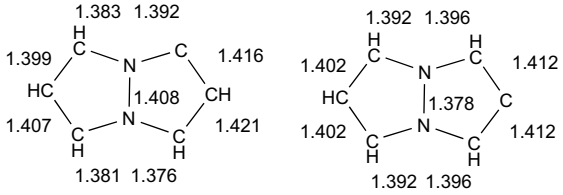

Scheme 8. Optimized geometry of the protonated structures at the MP2/6-311++G(d,p) computational level.

Table 3
Protonation energies

Atom	B3LYP/6-311++G(d,p)			MP2/6-311++G(d,p)		
Prot. atom	E_{total} (hartree)	E_{rel} (kJ mol^{-1})	Prot. energy (kJ mol^{-1})	E_{rel} (kJ mol^{-1})	Prot. energy (kJ mol^{-1})	E_{rel} (kJ mol^{-1})
C1	−342.152863	0.00	−1034.2	−341.157846	0.00	−1019.8
C2	−342.0848174	178.65	−855.5	−341.088927	180.95	−838.8
N	−342.0365068	305.49	−728.7	−341.043254	300.86	−718.9

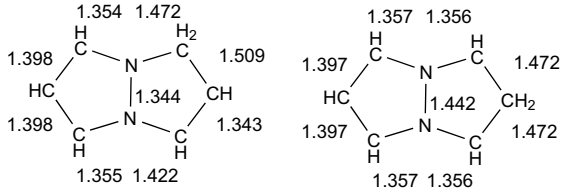

Scheme 6. Bond distances of the protonated molecules calculated at the MP2/6-311++G(d,p) computational level.

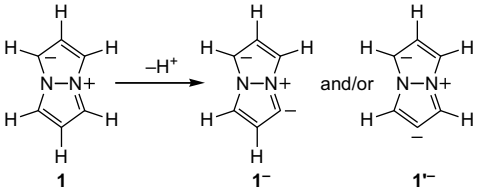

Scheme 7. Deprotonation of **1**.

The NICS(1) values of the rings drops to −2.53 and −6.76 in the C1 and C2 protonated molecules while the non-protonated ring shows values closer to those obtained in the neutral molecule (−10.25 and −7.68, respectively).

The NICS(1) values of the ring where the deprotonation occurs, slightly increases versus that of the neutral system (−11.69 and −11.03 in the C1 and C2 deprotonated structures) and the unaltered ring shows a value of −7.08 for the two systems studied.

2.5. Hydrogen bonds

2.5.1. 3a,6a-Diazapentalene as HB acceptor

The complexes formed by **1** with four hydrogen bond donors (HNC, HCN, HF, and H_2O) have been optimized. The minima show a disposition of the HB donors pointing toward the CC bonds (Fig. 6) as expected based on the presence of a minimum of the MEP on that region as previously indicated. In the strongest complexes, the interacting hydrogen is closer to C1 than C2 while in the weakest, the opposite happens. In the case of the complex $\mathbf{1}/H_2O$, two symmetrical interactions (H···C1 and H···C6) are obtained (Fig. 6).

The B3LYP computational level provides shorter interatomic distances, except for the $\mathbf{1}/H_2O$ complex, and smaller interaction energies (Table 5) than those obtained for the corresponding MP2 complexes. The failure of the B3LYP to properly characterize weak interactions has been associated to its poor description of disperse forces that become very important in these cases. At the MP2 level, the stronger complex is obtained with the HNC molecule followed by the HCN, being those of HF and H_2O of similar stability.

Table 4
Deprotonation energies at the B3LYP/6-311++G(d,p) and MP2/6-311++G(d,p) levels

Atom	B3LYP/6-311++G(d,p)			MP2/6-311++G(d,p)		
	E_{total} (hartree)	E_{rel} (kJ mol^{-1})	Deprot.	E_{total} (hartree)	E_{rel} (kJ mol^{-1})	Deprot.
C1	−341.1343222	0.00	1640.0	−340.147548	0.00	1632.8
C2	−341.1211587	34.56	1674.6	−340.135219	32.37	1665.1

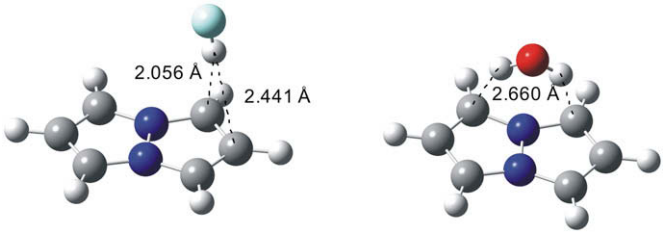

Figure 6. Optimized geometries of the **1**/HF and **1**/H_2O complexes at the MP2/6-311++G(d,p) computational level.

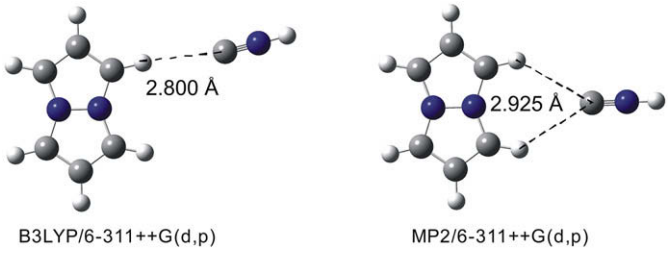

Figure 7. Optimized geometry of the **1**/CNH (C1) complex at B3LYP/6-311++G(d,p) and MP2/6-311++G(d,p) computational levels.

Table 5
Interaction energy (kJ mol^{-1}) and intermolecular distance (Å), for the hydrogen complexes studied

Complex	Symmetry	B3LYP/6-311++G(d,p)		MP2/6-311++G(d,p)	
		E_I	H···C1 dist.	E_I	H···C1 dist.
1/HNC	C_1	−18.29	2.222	−37.10	2.236
1/HCN	C_1	−11.60	2.568	−29.16	2.657
1/HF	C_1	−24.94	2.006	−27.32	2.056
1/H_2O	C_s	−12.31	2.721[a]	−27.33	2.660[a]

[a] Two identical H···C interactions are observed.

Table 7
Interaction energy (kJ mol^{-1}) and interatomic distances (Å)

Complex	Symmetry	B3LYP/6-311++G(d,p)		MP2/6-311++G(d,p)	
		E_I	HB distance	E_I	Distance
1/CNH (C1)	C_s	−4.55	2.799	−10.34	2.925[a]
1/CNH (C2)	C_{2v}	2.86	2.883	−6.66	2.753
1/NCH (C1)	C_s	5.17	2.635	−11.70	2.711/2.718[b]
1/NCH (C2)	C_{2v}	−3.32	2.695	−6.92	2.588

[a] Two identical interactions with C1–H and C6–H.
[b] Distances to C1H and C6H, respectively.

The analysis of the electron density shows three different bonding patterns for the complexes studied here. Thus, the **1**/HF and **1**/HNC complexes show a unique bond path between the C1 and the hydrogen bond donor molecule. The **1**/HCN complex shows a bond path between C2 and the hydrogen atom of HCN and two bond paths between N4 and N8 and the carbon atom of HCN and finally, the **1**/H_2O complex shows two bonds that links the oxygen atom with N4. In all the cases, the values of the electron density and electron density at the bond critical point (bcp) are positive and small (Table 6) as described for other hydrogen bonded systems.[28] The calculated charge within the AIM methodology shows a charge transfer between 0.051 and 0.017*e* from **1** to the HB donor. The volume contraction upon complexation compared to those of the isolated monomers varies between 20 and 28 a.u.

Table 6
Properties of the HB bcp (a.u.), charge transfer (*e*), and variation of the total volume (a.u.) upon complexation calculated at the MP2/6-311++G(d,p) computational level

Complex	ρ_{bcp}	$\nabla^2\rho_{bcp}$	Charge transfer	Δ Volume
1/HNC	0.012	0.053	−0.040	−28.28
1/HCN	0.010	0.034	−0.026	−27.56
1/HF	0.024	0.061	−0.051	−20.37
1/H_2O	0.008[a]	0.032	−0.017	−22.74

[a] Two identical bcp are obtained.

2.5.2. 3a,6a-Diazapentalene as HB donor

The possibility that the acidic hydrogen atoms of **1** can act as hydrogen bond donors has been explored using the NCH and CNH molecules as model of HB acceptors. Two minima have been located for each HB acceptor, one where the interacting group of **1** is the C1–H, and another where it interacts with the C2–H. In the first case, the geometrical disposition obtained depends on the computational method used (Fig. 7). Thus, at B3LYP level a linear HB is formed while at MP2 level the HB acceptor interacts simultaneously with C1–H and C6–H. As previously, the B3LYP interaction energies are much smaller than those obtained at the MP2 level (Table 7). The most stable complex corresponds to that where the interaction is established with the C1–H moiety of **1**, in good agreement with the larger acidity of this group shown previously.

The analysis of the electron density shows a unique intermolecular bcp between the HB acceptors and the C2–H and a bifurcated hydrogen bond in the complexes with C1–H and C6–H. The values (Table 8) obtained, derived from the AIM analysis, are smaller than those for the complexes where **1** acts as HB acceptor as an additional indication that these complexes are weaker than those discussed previously. It is worth mentioned that the volume reduction is larger in the complexes with C2 that in those with C1.

Table 8
Properties of the HB bcp (a.u.), charge transfer (*e*), and variation of the total volume (a.u.) upon complexation calculated at the MP2/6-311++G(d,p) computational level

Complex	ρ_{bcp}	$\nabla^2\rho_{bcp}$	Charge transfer	Δ Volume
1/CNH (C1)	0.005[a]	0.014	0.009	1.33
1/CNH (C2)	0.006	0.018	0.007	−0.31
1/NCH (C1)	0.006	0.020	0.004	−3.90
1/NCH (C2)	0.007	0.023	0.003	−4.83

[a] Two identical bcp are obtained.

2.6. Interaction with charged species (cations and anions)

A unique minimum is found in the complexes between **1** and the alkaline cations (Fig. 8). While in the case of the lithium and sodium complexes a C_s symmetry is observed with the metallic atoms interaction with C_2, a C_{2v} symmetry is observed for the potassium case being in this case the interaction with the nitrogen atoms. The interaction energy of the complexes (Table 9) decreases as the size of the cation increases, an indication that the main attractive force of the interaction is electrostatic. Thus, the smaller cations, are closer to **1**, showing a more effective electrostatic interaction.

A catastrophic situation should be obtained for a disposition of the metal atom intermediate between that found for the Na and K with a simultaneous formation of three bcp between the cations and the C2, N4, and N8. The small values of the electron density and its Laplacian (Table 10) are indicative of the closed shell interaction between the cations that remain with a charge closed to +1.0*e* and the neutral system **1**. The larger charge transfer corresponds for the lithium complex followed by the potassium one being the smallest in the sodium one case. The volume variation is similar to those described for the hydrogen bonded complex of **1** with HB donors.

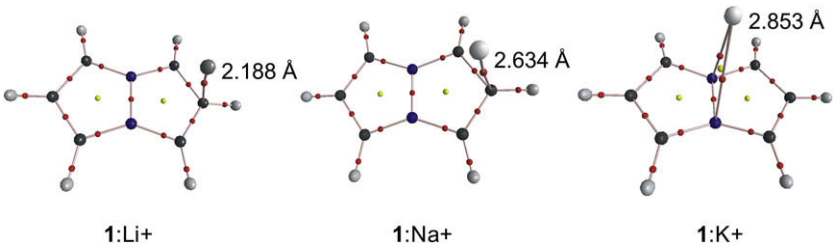

Figure 8. Molecular graph of the complexes between the alkaline cations and **1** at the MP2/6-311++G(d,p) computational level. The interatomic distance between the cation and the interacting atoms are shown. The bond and ring critical point are shown with red and yellow dots, respectively. The lines connecting the atoms represent the bond path.

Table 9
Interaction energies (kJ mol^{-1}) and intermolecular distances (Å) in the complexes with cations

Complex	Symmetry	B3LYP/6-311++G(d,p)		MP2/6-311++G(d,p)	
		E_I	Dist.	E_I	Dist.[a]
1/Li$^+$	C_s	−164.69	2.151	−158.92	2.188
1/Na$^+$	C_s	−106.73	2.561	−100.59	2.634
1/K$^+$	C_{2v}	−75.72	2.878	−93.57	2.853

[a] The tabulated distance corresponds to the one between the cation and the carbon atoms connected via a bond path in the AIM analysis.

Table 10
Properties of the intermolecular bcp (a.u.), charge of the cation (e), variation of the volume calculated at the MP2/6-311++G(d,p) computational level

Complex	ρ_{bcp}	$\nabla^2\rho_{bcp}$	Charge cation	Δ Volume
1/Li$^+$	0.022	0.127	0.929	−14.26
1/Na$^+$	0.014	0.070	0.946	−13.42
1/K$^+$	0.014	0.007	0.935	−33.54

Two minima have been found between anions (F$^-$, Cl$^-$, and Br$^-$) and **1**, interacting with the C2–H moieties and another one interacting simultaneously with C1–H and C6–H (Fig. 9). For the three anions, the second configuration is more stable than the first one. For a given anion, the interatomic distances are shorter for those cases where the interaction is with one CH group than with two. As previously commented for the case of the interaction with cations, the size of the anion determines the intermolecular distance, shorter for the smaller anions, and the interaction energy, smaller as the size of the cation increases for each minima configuration studied. Those configurations where the anion interacts with two hydrogen atoms are more stable that the ones when the same anion interacts with only one. However, the interaction energy in the most stable configuration is less than twice in the less stable one, an indication that in the former the interaction energy is maximizing and not the individual contacts in a similar fashion of what has been described for bifurcated hydrogen bonds (Table 11).[29]

The analysis of the electron density shows a single intermolecular bcp in the complexes with C2–H while two are obtained in the case of the simultaneous interaction with C1–H and C6–H (Table 12). The values of the electron density and Laplacian are consistent with the range described for hydrogen bonds. As expected with the observed intermolecular and in agreement with previous reports,[30,31] the shorter the intermolecular distance, the larger are the values obtained for the electron density and the corresponding Laplacian. In the complexes of chloride and bromide, the interactions with two hydrogen atoms are associated with a larger charge transfer from the anion to **1** than in those cases where the interaction is with one hydrogen atom while in the fluoride complex the opposite is observed. A larger volume reduction is observed in the complexes that interact with C1–H and C6–H simultaneously than in those complexes where the interaction is only with C2–H.

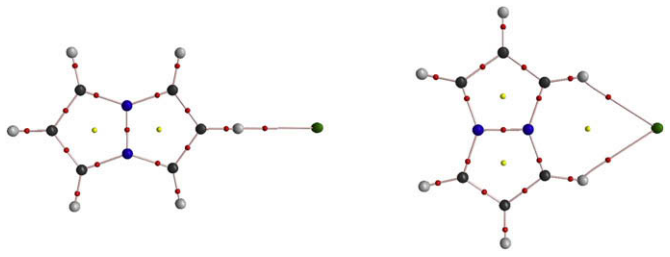

Figure 9. Molecular graph of the optimized complexes of **1**/Cl$^-$ at the MP2/6-311++G(d,p) computational level.

Table 11
Interaction energies (kJ mol^{-1}) and interatomic distances (Å) with anions

Complex	Symmetry	B3LYP/6-311++G(d,p)		MP2/6-311++G(d,p)	
		E_I	Distance X···H	E_I	Distance X···H
1/F$^-$ (C2–H)	C_{2v}	−71.12	1.601	−69.13	1.568
1/F$^-$ (C1–H, C6–H)	C_{2v}	−88.96	1.995	−90.13	1.993
1/Cl$^-$ (C2–H)	C_{2v}	−28.86	2.447	−40.31	2.377
1/Cl$^-$ (C1–H, C6–H)	C_{2v}	−43.74	2.683	−61.17	2.581
1/Br$^-$ (C2–H)	C_{2v}	−22.65	2.683	−34.09	2.597
1/Br$^-$ (C1–H, C6–H)	C_{2v}	−35.26	2.894	−53.19	2.768

Table 12
Properties of the intermolecular bcp (a.u.), charge of the anions (e), variation of the calculated at the MP2/6-311++G(d,p) computational level

Complex	ρ_{bcp}	$\nabla^2\rho_{bcp}$	Charge cation	Δ Volume
1/F$^-$ (C2–H)	0.058	0.168	−0.924	−24.09
1/F$^-$ (C1–H, C6–H)	0.024	0.085	−0.940	−29.54
1/Cl$^-$ (C2–H)	0.018	0.052	−0.953	−31.27
1/Cl$^-$ (C1–H, C6–H)	0.013	0.039	−0.934	−39.17
1/Br$^-$ (C2–H)	0.014	0.037	−0.956	−0.45
1/Br$^-$ (C1–H, C6–H)	0.011	0.030	−0.936	−18.30

3. Conclusions

The main conclusions of the present study are:

1. A theoretical study of the properties of the 3a,6a-diazapentalene **1** has been carried out by means of DFT and ab initio methods [B3LYP/6-311++G(d,p) and MP2/6-311++G(d,p)]. The molecular electrostatic potential of this compound shows negative regions surrounding the carbon atoms while around the nitrogen ones the value of the electrostatic potential is positive, opposite to the general rule.
2. When reported, the calculations reproduce adequately the UV, IR, and NMR spectra, thus allowing calculated unreported properties to be considered as reliable.

3. The barrier of the ring-ring isomerism has been evaluated at 175 kJ mol^{-1}, the eight-member ring isomer being 34 kJ mol^{-1} less stable than **1** at the MP2/6-311++G(d,p) level.
4. The most favorable protonation and deprotonation place is the C1 in both cases.
5. The 3a,6a-diazapentalene seems to be a better HB acceptor than a HB donor based on the interaction energies of the complexes calculated here. A similar trend is observed in its interaction with ions, since the complexes formed with the alkaline cations are stronger than those complexes with the halogen anions.

4. Methods

The geometry of the systems has been fully optimized with the hybrid HF/DFT B3LYP[32,33] and the MP2[34] computational methods using the 6-311++G(d,p) basis set.[35] In all cases, the geometries obtained have been confirmed to be energetic minima by frequency calculation at both computational level. The frequency calculations have been used in addition, to obtain the harmonic vibrational frequencies. The UV spectrum has been obtained using the time-dependent DFT (TD-DFT) computational method[36] at the B3LYP/6-311++G(d,p) level.

The Natural Resonance Theory (NRT)[37] based on the Natural Bond Orbital (NBO) method[38] has been used to evaluate the weight of the different resonance Lewis forms that contribute to the structure of the molecule. These calculation has been carried with the NBO-5G code[39] within the Gamess program.[40]

The electron density has been analyzed within the Atoms In Molecules (AIM) methodology[41] using the PROAIMV,[42] AIM2000,[43] and AIMAll programs.[44] The atomic properties (volume and charge) have been evaluated by the integration of the electron density within the atomic basins. The integrated Laplacian has been taken as an initial measure of the quality of the integration. Ideally, the Laplacian as integrated over any atomic basins of a system should result in a null value; however, values smaller than 1×10^{-3} have been shown to provide only negligible errors in the results.[45] Thus, the conditions of the integration have been adjusted when this requirement was not satisfied. The 0.001 a.u. isosurface has been used to evaluate the atomic volume since this value has been recommended to reproduce the van der Waals volume.[41]

The Electron Localization Function (ELF)[46] has been evaluated with the TopMod program.[47]

Acknowledgements

This work was carried out with financial support from the Ministerio de Ciencia y Tecnología (Project No. CTQ2006-14487-C02-01/BQU) and Comunidad Autónoma de Madrid (Project MADRISOLAR, ref. S-0505/PPQ/0225). Thanks are given to the CTI (CSIC) for allocation of computer time.

Supplementary data

Optimized geometry of thecomplexes considered in the present article at the MP2/6-311++G(d,p) computational level. Supplementary data associated with this article can be found in the online version, at doi:10.1016/j.tet.2009.05.017.

References and notes

1. *Chem. Abstr.* **1972–1976**, 9th Collective Index, 33454CS.
2. Elguero, J.; Claramunt, R. M.; Summers, A. J. H. *Adv. Heterocycl. Chem.* **1978**, *22*, 183–320 (see pages 262 and 293).
3. Katritzky, A. R.; Rees, C. W. *Comprehensive Heterocyclic Chemistry*; Pergamon: Oxford, 1984; Vol. 8, p 48.
4. Ramsden, C. A. *Tetrahedron* **1977**, *33*, 3193–3202.
5. (a) Solomons, T. W. G.; Fowler, F. W. *Chem. Ind. (London)* **1963**, 1462–1464; (b) Solomons, T. W. G.; Fowler, F. W.; Calderazzo, J. *J. Am. Chem. Soc.* **1965**, *87*, 528–531; (c) Solomons, T. W. G.; Voigt, C. F. *J. Am. Chem. Soc.* **1965**, *87*, 5256–5256; (d) Solomons, T. W. G.; Voigt, C. F. *J. Am. Chem. Soc.* **1966**, *88*, 1992–1994.
6. (a) Trofimenko, S. *J. Am. Chem. Soc.* **1965**, *87*, 4393–4394; (b) Trofimenko, S. *J. Am. Chem. Soc.* **1966**, *88*, 5588–5592.
7. Claramunt, R. M.; Trofimenko, S.; Rozas, I.; Elguero, J. *Spectrosc.* **1996/1997**, *13*, 113–123.
8. Matsumoto, K.; Uchida, T. *Chem. Lett.* **1978**, 1093–1094.
9. Matsumoto, M.; Iida, H.; Hinomoto, T.; Uchida, T. *J. Chem. Res., Synop.* **1995**, 338–339.
10. Matsumoto, M.; Iida, H.; Katsura, H.; Machiguchi, T.; Uekusa, H.; Ohashi, Y. *J. Chem. Soc., Perkin Trans. 1* **1996**, 2333–2335.
11. Galasso, V.; De Alti, G. *Theor. Chem. Acc.* **1968**, *11*, 411–416.
12. Chuiguk, V. A. *Chem. Heterocycl. Compd.* **1983**, *19*, 1–13.
13. Allen, F. H. *Acta Crystallogr.* **2002**, *B58*, 380–388; Allen, F. H.; Motherwell, W. D. S. *Acta Crystallogr.* **2002**, *B58*, 407–422, CSD database version 5.30 (November 2008).
14. Silvi, B.; Fourre, I.; Alikhani, M. E. *Monatsh. Chem.* **2005**, *136*, 855–879.
15. Callahan, M. P.; Crews, B.; Abo-Riziq, A.; Grace, L.; de Vries, M. S.; Gengeliczki, Z.; Holmes, T. M.; Hill, G. A. *Phys. Chem. Chem. Phys.* **2007**, *9*, 4587–4591.
16. Andersson, M. P.; Uvdal, P. *J. Phys. Chem. A* **2005**, *109*, 2937–2941.
17. Cavero, E.; Giménez, R.; Uriel, S.; Beltrán, E.; Serrano, J. L.; Alkorta, I.; Elguero, J. *Cryst. Growth Des.* **2008**, *8*, 838–847.
18. Blanco, F.; Alkorta, I.; Elguero, J. *Magn. Reson. Chem.* **2007**, *45*, 797–800.
19. Schleyer, P. v. R.; Maerker, C.; Dransfeld, A.; Jiao, H.; Hommes, N. v. E. *J. Am. Chem. Soc.* **1996**, *118*, 6317–6318.
20. Alkorta, I.; Blanco, F.; Elguero, J. *J. Mol. Struct. Theochem.* **2008**, *851*, 75–83.
21. Alkorta, I.; Blanco, F.; Elguero, J. *Tetrahedron* **2008**, *64*, 3826–3836.
22. Alkorta, I.; Blanco, F.; Elguero, J. *J. Phys. Chem. A* **2008**, *112*, 1817–1822.
23. Perlmutter, H. D. *Adv. Heterocycl. Chem.* **1989**, *46*, 1–72.
24. Doxsee, K. M. In *Comprehensive Heterocyclic Chemistry II*; Katritzky, A. R., Rees, C. W., Scriven, E. F. V., Eds.; Eight-membered Rings with Two Heteroatoms 1,5; Elsevier: Oxford, 1996; Vol. 9, pp 591–650.
25. Alkorta, I.; Picazo, O.; Elguero, J. *J. Phys. Chem. A* **2006**, *110*, 2259–2268.
26. Gompper, R.; Noth, H.; Rattay, W.; Schwarzensteiner, M. L.; Spes, P.; Wagner, H. U. *Angew. Chem., Int. Ed. Engl.* **1987**, *26*, 1039–1041.
27. Enjalbal, C.; Aubagnac, J. L.; Trofimenko, S.; Claramunt, R.; Sanz, D.; Elguero, J. *J. Heterocycl. Chem.* **1998**, *35*, 1405–1412.
28. Alkorta, I.; Rozas, I.; Elguero, J. *Chem. Soc. Rev.* **1998**, *27*, 163–170.
29. Rozas, I.; Alkorta, I.; Elguero, J. *J. Phys. Chem. A* **1998**, *102*, 9925–9932.
30. Alkorta, I.; Barrios, L.; Rozas, I.; Elguero, J. *J. Mol. Struct. (Theochem)* **2000**, *496*, 131–137.
31. Mata, I.; Alkorta, I.; Espinosa, E.; Molins, E.; Elguero, J. Topological Properties of the Electron Distribution in Hydrogen Bonded Systems. In *The Quantum Theory of Atoms in Molecules*; Matta, C. F., Boyd, R. J., Eds.; Wiley-VCH: Weinheim, 2007.
32. Becke, A. D. *J. Chem. Phys.* **1993**, *98*, 5648–5652.
33. Lee, C.; Yang, W.; Parr, R. G. *Phys. Rev. B* **1988**, *37*, 785–789.
34. Møller, C.; Plesset, M. S. *Phys. Rev.* **1934**, *46*, 618–622.
35. Frisch, M. J.; Pople, J. A.; Krishnam, R.; Binkley, J. S. *J. Chem. Phys.* **1984**, *80*, 3265–3269.
36. Stratmann, R. E.; Scuseria, G. E.; Frisch, M. J. *J. Chem. Phys.* **1998**, *109*, 8218–8224.
37. Glendening, E. D.; Weinhold, F. *J. Comput. Chem.* **1998**, *19*, 593–609.
38. Weinhold, F.; Landis, C. R. *Valency and Bonding. A Natural Bond Orbital Donor-Acceptor Perspective*; Cambridge Press: Cambridge, 2005.
39. Badenhoop, J. K.; Reed, A. E.; Carpenter, J. E.; Bohmann, J. A.; Morales, C. M.; Weinhold, F. *NBO 5.G.E.D. Glendening*; Theoretical Chemistry Institute, University of Wisconsin: Madison, WI, 2004.
40. Gamess Version 11 Schmidt, M. W.; Baldridge, K. K.; Boatz, J. A.; Elbert, S. T.; Gordon, M. S.; Jensen, J. H.; Koseki, S.; Matsunaga, N.; Nguyen, K. A.; Su, S. J.; Windus, T. L.; Dupuis, M.; Montgomery, J. A. *J. Comput. Chem.* **1993**, *14*, 1347–1363.
41. Bader, R. F. W. Atoms in Molecules: A Quantum Theory. In *The International Series of Monographs of Chemistry*; Halpen, J., Green, M. L. H., Eds.; Clarendon: Oxford, 1990.
42. Bieger-König, F. W.; Bader, R. F. W.; Tang, T. H. *J. Comput. Chem.* **1982**, *3*, 317–328.
43. Biegler-König, F. W; Schönbom, J. *AIM2000*, 2nd ed; Büro Für Innovative Software: Bielefeld, Germany, 2002.
44. Keith, T. A. AIMAll program (Version 08.11.29), 2008 (aim.tkgristmill.com).
45. Alkorta, I.; Picazo, O. *ARKIVOC* **2005**, *ix*, 305–320.
46. Becke, A. D.; Edgecombe, K. E. *J. Chem. Phys.* **1990**, *92*, 5397–5403; Silvi, B.; Savin, A. *Nature* **1994**, *371*, 683–689.
47. Noury, S.; Krokidis, X.; Fuster, F.; Silvi, B. *TopMod Package*; Universite Pierre et Marie Curie: Paris, 1997; *Comput. Chem.* **1999**, *23*, 597.